Hydrogen Production Using Nickel Electrocatalysts with Pendant Amines: Ligand Effects on Rates and Overpotentials

ARTICLE *in* ACS CATALYSIS · NOVEMBER 2013

Impact Factor: 9.31 · DOI: 10.1021/cs400638f

ACS Catalysis

Research Article

pubs.acs.org/acscatalysis

Hydrogen Production Using Nickel Electrocatalysts with Pendant Amines: Ligand Effects on Rates and Overpotentials

Stefan Wiese, Uriah J. Kilgore, Ming-Hsun Ho, Simone Raugei, Daniel L. DuBois, R. Morris Bullock, and Monte L. Helm*

Center for Molecular Electrocatalysis, Pacific Northwest National Laboratory, Richland, Washington 99352, United States

Supporting Information

ABSTRACT: A Ni-based electrocatalyst for H_2 production, $[Ni(8P^{Ph}{}_2N^{C_6H_4Br})_2](BF_4)_2$, featuring eight-membered cyclic diphosphine ligands incorporating a single amine base, 1-*para*-bromophenyl-3,7-triphenyl-1-aza-3,7-diphosphacycloheptane ($8P^{Ph}{}_2N^{C_6H_4Br}$) has been synthesized and characterized. X-ray diffraction studies reveal that the cation of $[Ni(8P^{Ph}{}_2N^{C_6H_4Br})_2(CH_3CN)](BF_4)_2$ has a distorted trigonal bipyramidal geometry. In CH_3CN, $[Ni(8P^{Ph}{}_2N^{C_6H_4Br})_2]^{2+}$ is an electrocatalyst for reduction of protons, and it has a maximum turnover frequency for H_2 production of 800 s^{-1} with a 700 mV overpotential (at $E_{cat/2}$) when using [(DMF)H]OTf as the acid. Addition of H_2O to acidic CH_3CN solutions of $[Ni(8P^{Ph}{}_2N^{C_6H_4Br})_2]^{2+}$ results in an increase in the turnover frequency for H_2 production to a maximum of 3300 s^{-1} with an overpotential of 760 mV at $E_{cat/2}$. Computational studies carried out on $[Ni(8P^{Ph}{}_2N^{C_6H_4Br})_2]^{2+}$ indicate the observed catalytic rate is limited by formation of nonproductive protonated isomers, diverting active catalyst from the catalytic cycle. The results of this research show that proton delivery from the exogenous acid to the correct position on the proton relay of the metal complex is essential for fast H_2 production.

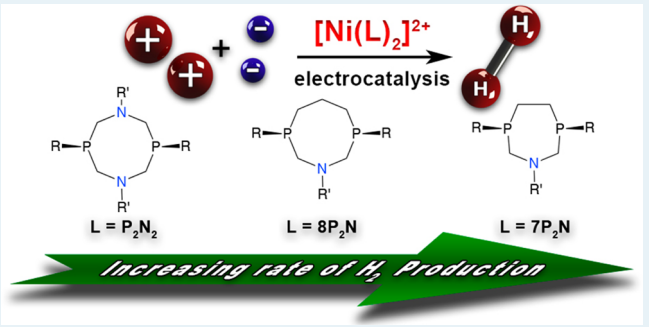

KEYWORDS: *hydrogen production, electrocatalysis, nickel phosphine complexes, pendant amines, proton relay, proton reduction*

INTRODUCTION

The development of renewable energy sources is essential for the world's future energy landscape, in part due to mitigating increasing CO_2 concentrations in the atmosphere resulting from the combustion of fossil fuels.[1] To make alternative energy solutions more competitive compared with existing energy sources, the challenge of reversible energy storage and delivery must be solved to address fluctuating energy supply and demand. Storage of electrical energy in chemical bonds is attractive because of the high energy density by weight of chemical fuels. One of the simplest reactions for storage of renewable energy is the formation of H_2 from two protons and two electrons. Platinum is an excellent catalyst for both production and oxidation of H_2, but its high cost and low abundance present problems for making catalysts based on precious metals economically competitive on a global scale. The use of earth-abundant metals for heterogeneous H_2 production has been well studied;[2−6] however, their use as homogeneous catalysts has only more recently been intensely studied.[7−10]

Nature provides remarkable examples of catalysts that use earth-abundant metals (Ni or Fe) for the production and oxidation of H_2: the hydrogenase enzymes catalyze H_2 production and oxidation efficiently and reversibly. For example, the [FeFe]-hydrogenase enzyme can both produce and oxidize H_2 at turnover frequencies of ≥9000 s^{-1} (Figure 1a).[11−14] Unfortunately, the limited long-term stability of

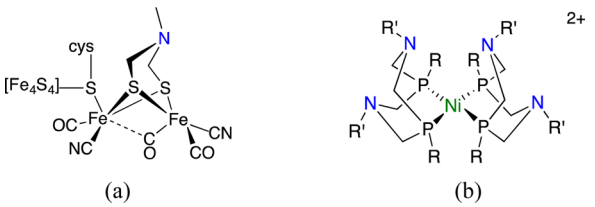

Figure 1. (a) Proposed catalytic site of [FeFe]-hydrogenase enzyme. (b) General structure of $[Ni(P^R{}_2N^R{}_2)_2]^{2+}$ complexes.

hydrogenase enzymes outside of their native environment prevents their use for practical applications. Nonetheless, these enzymes teach the invaluable lesson of combining pendant bases that function as proton relays (Figure 1, highlighted in blue) with earth-abundant metals for fast, efficient H_2 production and oxidation.[15−18] Many synthetic mimics of the hydrogenase enzymes that incorporate a base in the second coordination sphere have been reported.[19−26] Complexes using nickel,[27−29] cobalt,[30−33] iron,[34−40] and molybdenum[41−43] have been shown to be electrocatalysts for production or oxidation of H_2.

Received: August 2, 2013
Revised: September 20, 2013

   dx.doi.org/10.1021/cs400638f | ACS Catal. 2013, 3, 2527−2535

An extensive series of $[Ni(P^{R}_{2}N^{R'}_{2})_2]^{2+}$ complexes (Figure 1b) have been studied in our laboratory as functional models of catalysis by the hydrogenase enzymes. Depending on the R and R′ substituents, these catalysts function for H_2 production or oxidation or for bidirectional catalysis (Figure 1).[27,28] Intra- and intermolecular proton movement is facilitated by the pendant amines in the second coordination sphere.[44,45] Mechanistic and computational investigations suggest that the H−H bond formation proceeds by nickel donating a hydride and a protonated pendant amine donating a proton.[44−46] Each pendant amine has two possible sites for protonation: positioned on the side nearest the metal center, referred to as endo (Figure 2a), or the side of the N-atom pointing away from

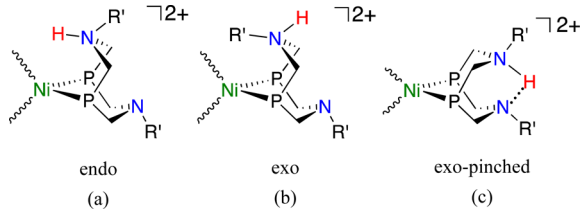

Figure 2. Depiction of singly protonated Ni(I) species resulting from protonation of the $[Ni(P^{R}_{2}N^{R'}_{2})_2]^{+}$ complexes. Second $P^{R}_{2}N^{R'}_{2}$ ligand not shown. (a) Endo with respect to the metal center, (b) exo with respect to the metal center, and (c) exo pinched protonation. For clarity, substituents on P are not shown.

the metal center, referred to as exo (Figure 2b). When protonation occurs in an exo position, chair-boat isomerization of the six-membered chelate ring results in species in which a proton is "pinched" between two pendant amines with a NH··· N hydrogen bond (Figure 2c). Since catalytic formation of H_2 with the $[Ni(P^{R}_{2}N^{R'}_{2})_2]^{2+}$ complexes requires two protons, only the isomer that has both protons in an endo position is productive for hydrogen evolution.[27,28] Previous experimental and computational studies have shown that exo protonation is typically the kinetic and thermodynamic product (Figure 2b/c), leading to the conclusion that only a fraction of the catalyst is present in the correct isomeric configuration to produce H_2 under electrocatalytic conditions.[8,44−47]

To avoid the exo pinched protonated species, a new class of H_2 production Ni(II) electrocatalysts, $[Ni(7P^{R}_{2}N^{R'})_2]^{2+}$, was synthesized (Figure 3a).[8,48] Although exo protonation is still possible, removal of one of the pendant amines from the ligand precludes formation of an exo pinched species (Figure 3c).

The $[Ni(7P^{Ph}_{2}N^{Ph})_2]^{2+}$ complex achieved the fastest electrocatalytic H_2 production rates yet reported, exceeding 100 000 s^{-1} at 22 °C, about an order of magnitude faster than the [FeFe]-hydrogenase enzyme.[48] The very high rates for H_2 production of the $[Ni(7P^{Ph}_{2}N^{C6H4X})_2]^{2+}$ complexes, however, occur at the cost of overpotential. Computational studies

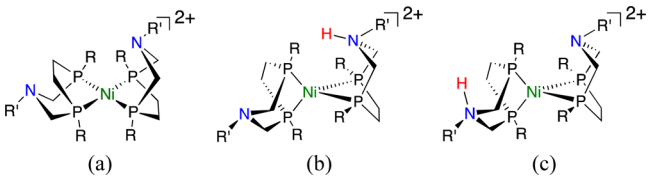

Figure 3. Depiction of (a) $[Ni(7P^{R}_{2}N^{R'})_2]^{2+}$ (b) endo protonated Ni(I) isomer $[Ni(7P^{R}_{2}N^{R'}H)(7P^{R}_{2}N^{R'})]^{2+}$ (c) exo protonated Ni(I) isomer $[Ni(7P^{R}_{2}N^{R'}H)(7P^{R}_{2}N^{R'})]^{2+}$.

recently reported for a family of $[Ni(7P^{Ph}_{2}N^{C6H4X})_2]^{2+}$ catalysts have shown these complexes, with just one pendant amine in the ligand structure, results in stabilization of endo protonation relative to exo protonation, leading to faster catalytic rates.[8] We sought to synthesize a new catalyst that functions at a decreased overpotential while maintaining high turnover frequencies.[8,48−51] Modifying the P−M−P bite angle of the diphosphine ligands has been previously shown to change the Ni(II/I) couple of the complexes.[49,52−54] The effect on the Ni(II/I) couple is due to a distortion of the square-planar geometry of Ni(II) complex. As the bite angle increases, a greater distortion away from square-planar geometry occurs, resulting in a reduced antibonding overlap of the σ-orbital of the phosphine ligands and the d_{x2-y2} orbital of nickel. This decrease in electron density at nickel moves the Ni(II/I) couple to more positive potentials, resulting in lower overpotentials for H_2 production.[8,54,55]

We report here the synthesis and study of a H_2 production catalyst $[Ni(8P^{Ph}_{2}N^{C_6H_4Br})_2](BF_4)_2$ (abbreviated as $[Ni(8P_2N)_2]^{2+}$) that contains *only one* pendant amine on each ligand (Scheme 1), preventing formation of exo pinched

Scheme 1. Ligands Discussed in This Study

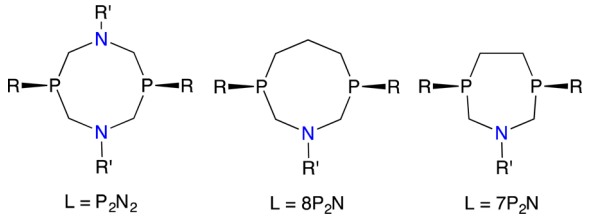

species that was observed in the previously reported $[Ni(P^{Ph}_{2}N^{C_6H_4Br}_{2})_2]^{2+}$ (abbreviated as $[Ni(P_2N_2)_2]^{2+}$) catalyst.[47] This study of $[Ni(8P_2N)_2]^{2+}$ also allows direct comparison of the of the ligand 8-membered chelate ring size relative to the previously reported $[Ni(7P^{Ph}_{2}N^{C_6H_4Br})_2]^{2+}$ complex with a 7-membered ring (abbreviated as $[Ni(7P_2N)_2]^{2+}$).[8]

RESULTS

Synthesis and Characterization of the $8P_2N$ Ligand and $[Ni(8P_2N)_2]^{2+}$. The synthesis of 1-aza-3,7-diphosphacyclooctanes has been described previously by Karasik et al. (eq 1).[56] Adapting their procedure to the synthesis of a similar 8-

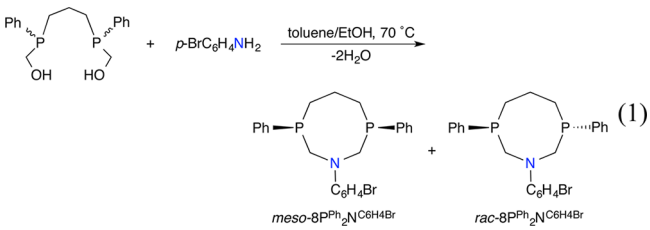

(1)

membered ring, the synthesis of 1-*para*-bromophenyl-3,7-triphenyl-1-aza-3,7-diphosphacyclooctane $(8P^{Ph}_{2}N^{C_6H_4Br})$ was accomplished through the addition of 1 equiv of *p*-bromoaniline to 1,3-bis(phenylhydroxymethyl-phosphino)propane in a 1:2 solvent mixture of toluene and ethanol. After an overnight reaction time at 70 °C, the $^{31}P\{^{1}H\}$ NMR spectrum of the reaction mixture showed formation of both the rac and meso isomers of $8P^{Ph}_{2}N^{C_6H_4Br}$. The meso isomer was isolated as a white solid and characterized by ^{1}H and $^{31}P\{^{1}H\}$ NMR and

dx.doi.org/10.1021/cs400638f | ACS Catal. 2013, 3, 2527−2535

mass spectrometry, all of which are consistent with the indicated structure. Then $[Ni(CH_3CN)_6](BF_4)_2$ was treated with 2 equiv of the *meso*-$8P^{Ph}{}_2N^{C_6H_4Br}$, and $[Ni(8P_2N)_2](BF_4)_2$ was isolated as a red solid in a 78% yield (eq 2).

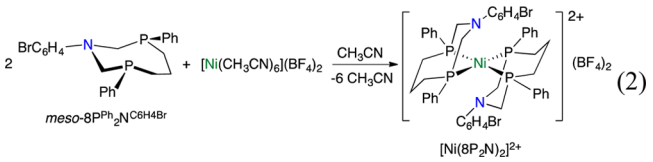

(2)

The $^{31}P\{^1H\}$ NMR spectrum of $[Ni(8P_2N)_2]^{2+}$ in CD_3CN at 25 °C shows a sharp peak at 4.2 ppm and two broad resonances at 20.1 and −11.6 ppm, all of similar intensities. The three peaks are attributed to the presence of two 5-coordinate isomers (Figure 4) in which CH_3CN functions as the fifth

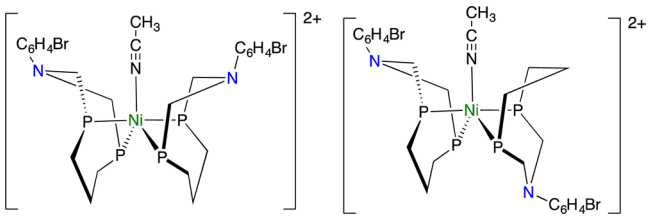

Figure 4. Proposed (a) up/up and (b) up/down isomers of $[Ni(8P_2N)_2CH_3CN]^{2+}$. Phenyl groups on the phosphorus atoms are omitted for clarity.

ligand, as seen in the $[Ni(7P_2N)_2(CH_3CN)]^{2+}$ complexes.[8,48] The sharp resonance at 4.2 ppm is attributed to the up/up isomer (Figure 4a) in which all phosphorus atoms are equivalent. The two broad resonances at 20.1 and −11.6 ppm correspond to the up/down isomer (Figure 4b) in which the two pairs of phosphorus atoms are inequivalent. At −30 °C, the resonance corresponding to the up/up isomer at 4.2 ppm remains unchanged, whereas the resonances for the up/down isomer at 20.1 and −11.6 ppm sharpen into an AA′XX′ pattern, supporting the assignment of the isomers.

Dark red crystals suitable for X-ray diffraction were grown from a solution of $[Ni(8P_2N)_2]^{2+}$ in CH_3CN layered with a small amount of diethyl ether. The resulting structure shows a 5-coordinate distorted trigonal bipyramidal species with two diphosphine ligands and an acetonitrile solvent molecule bound to nickel (Figure 5). The resulting isomer observed in this structure corresponds to the up/up isomer identified by NMR spectroscopy (Figure 4a). Each of the $8P^{Ph}{}_2N^{C_6H_4Br}$ ligands has Ni−P bond lengths ranging from 2.20 to 2.24 Å and P−Ni−P ligand bite angles of 82.55(4) and 83.07(4)°. Each diphosphine ligand forms two six-membered Ni-chelate rings, and similar to previously reported $[Ni(P_2N_2)_2(CH_3CN)]^{2+}$ structures, the rings on the side of the CH_3CN are in boat conformations, with the adjacent rings adopting chair conformations.[47,57] Complete crystallographic information is provided in the Supporting Information.

Electrochemical Studies. The cyclic voltammogram of $[Ni(8P_2N)_2]^{2+}$ shows two distinct and reversible reduction waves assigned to the Ni(II/I) and Ni(I/0) couples with $E_{1/2}$ values of −0.90 V (ΔE_p = 65 mV) and −1.10 V (ΔE_p = 67 mV), respectively, versus the Cp_2Fe^+/Cp_2Fe couple (Figure 6). A plot of the peak current of each reduction wave (i_p) vs the

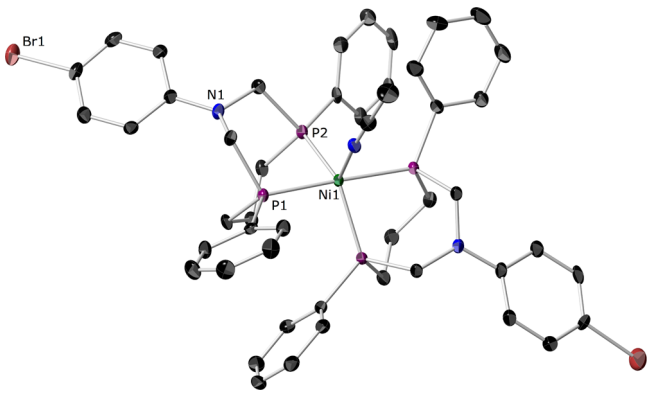

Figure 5. X-ray crystal structure of $[Ni(8P_2N)_2(CH_3CN)](BF_4)_2 \cdot 2CH_3CN$. The BF_4^- anions, CH_3CN solvent molecules, and H atoms have been omitted for clarity. Thermal ellipsoids are shown at the 50% probability level.

square root of the scan rate shows a linear correlation, implying diffusion-controlled electrochemical events.[58]

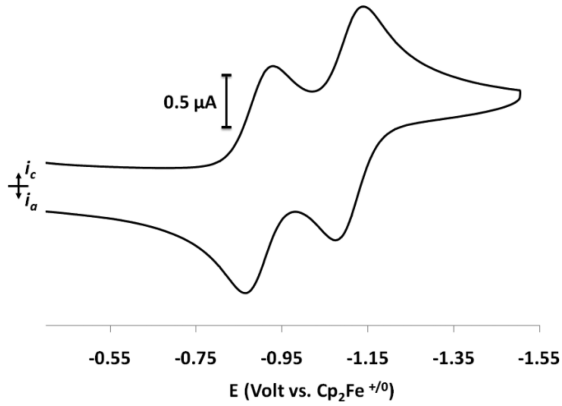

Figure 6. Cyclic voltammogram of 1.0 mM $[Ni(8P_2N)_2]^{2+}$ in 0.2 M $[Et_4N][BF_4]/CH_3CN$. Conditions: 1 mm glassy-carbon working electrode; scan rate = 0.1 V s^{-1} at 25 °C.

The $[Ni(8P_2N)_2]^{2+}$ complex is an active H_2 production catalyst using [(DMF)H]OTf (pK_a = 6.1 in CH_3CN)[59,60] as a Brønsted acid. The catalytic activity was measured from successive voltammograms of solutions in which the acid concentration was systematically increased until the catalytic current (i_{cat}) remained constant (acid concentration independent region). Figure 7a shows a typical series of voltammograms obtained with increasing acid concentration. Figure 7b shows that a plot of the catalytic current (i_{cat}) vs $[(DMF)H^+]^{1/2}$ is linear, then plateaus above 0.52 M $(DMF)H^+$, indicating the reaction is initially first-order with respect to acid concentration (i.e., eq 3, where n is the number of electrons involved in the catalytic reaction, F is Faraday's constant, A is the area of the electrode, D is the diffusion coefficient, k is the rate constant, and x is the order of the reaction with respect to acid). After a concentration of 0.7 M $(DMF)H^+$ is achieved, the reaction becomes pseudo-zero-order with respect to acid concentration.[61−64] Assuming that two electrons are passed for each H_2 molecule produced (n = 2) and the acid concentration does not change significantly during the course of the measurement (as indicated by a current plateau, i_{cat}), the catalytic rate constant (k_{obs}, eq 4), or turnover frequency (TOF), can be calculated

dx.doi.org/10.1021/cs400638f | ACS Catal. 2013, 3, 2527−2535

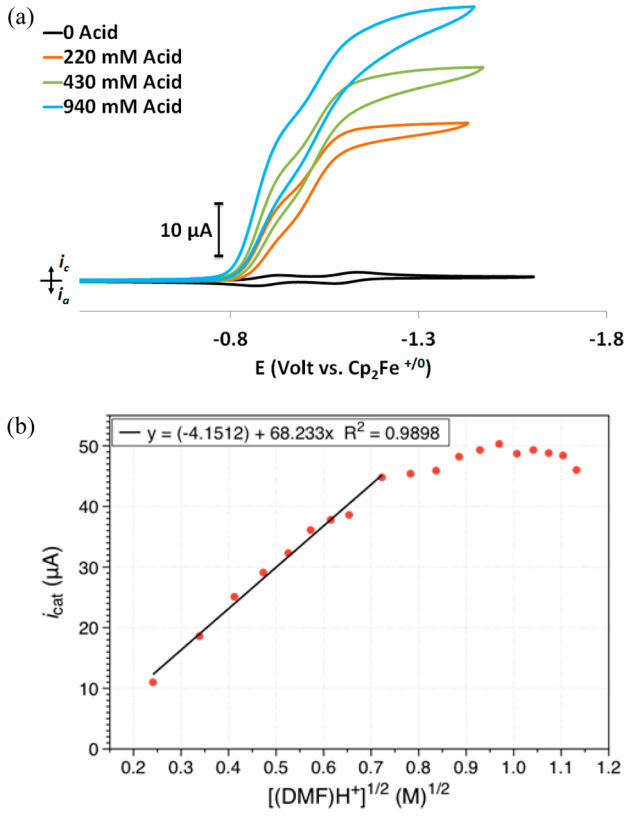

Figure 7. (a) Cyclic voltammograms of 0.44 mM $[Ni(8P_2N)_2]^{2+}$ in 0.20 M $[Bu_4N][PF_6]/CH_3CN$ with subsequent additions of $(DMF)H^+$. (b) Plot of i_{cat} vs $[(DMF)H^+]^{1/2}$. Conditions: 1 mm glassy-carbon working electrode; scan rate 0.1 V s^{-1} at 25 °C.

using eq 5 (υ = scan rate in V/s) or simplified eq 6 (T = 298 K).[58,62,63,65]

The potential (E_{cat}) at which i_{cat} was measured for each acid addition corresponds to the point where the catalytic waves first begin to plateau. The maximum TOF achieved for H_2 production with $[Ni(8P_2N)_2]^{2+}$ was observed to be 800 s^{-1} with ≥0.52 M $(DMF)H^+$. None of these molecular catalysts display linear Tafel-like behavior, in which the catalytic rate increases as the overpotential is increased, as is often observed in heterogeneous catalysis. For these molecular Ni electrocatalysts, the intrinsic electron transfer rate is likely much greater than the rate of catalysis.[58]

$$i_{cat} = nFA[cat]\sqrt{D(k[H^+]^x)} \quad (3)$$

$$k_{obs} = k[H^+]^x \quad (4)$$

$$\frac{i_{cat}}{i_p} = \frac{n}{0.4463}\sqrt{\frac{RTk_{obs}}{F\upsilon}} \quad (5)$$

$$k_{obs} = 1.94V^{-1}\cdot\upsilon\left(\frac{i_{cat}}{i_p}\right)^2 \quad (6)$$

To confirm H_2 production, a controlled potential coulometry experiment was performed using $[Ni(8P_2N)_2]^{2+}$ (0.17 mM) with the working electrode held at −1.40 V versus $Cp_2Fe^{+/0}$ in the presence of $(DMF)H^+$ (0.096 M); the average of three measurements resulted in a faradic current efficiency of 99 ± 5% with turnover numbers of 33, 58, and 77, confirming selective catalytic production of H_2.

In previous studies of $[Ni(P_2N_2)_2]^{2+}$ and $[Ni(7P_2N)_2]^{2+}$, H_2O was shown to significantly increase catalytic rates of production of H_2, so aliquots of H_2O were added subsequent to the acid additions for $[Ni(8P_2N)_2]^{2+}$ (Figure 8a).[8,47,66]

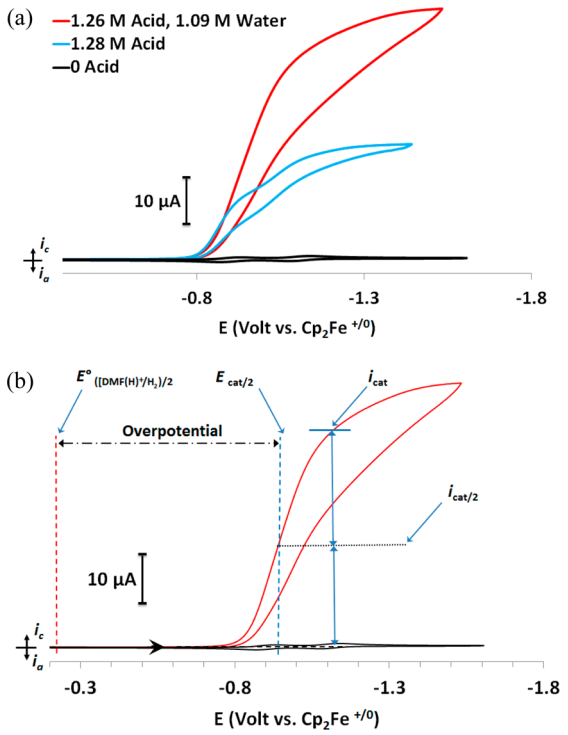

Figure 8. (a) Cyclic voltammograms of 0.44 mM $[Ni(8P_2N)_2]^{2+}$ in 0.20 M $[Bu_4N][PF_6]/CH_3CN$ with subsequent addition of $(DMF)H^+$, followed by H_2O. (b) Illustration of the overpotential determination. Conditions: 1 mm glassy-carbon working electrode; scan rate 0.1 V s^{-1} at 25 °C.

Addition of water up to 1.1 M to the reaction mixture containing 1.26 M $(DMF)H^+$ increased the current enhancement, resulting in a maximum turnover frequency of 3,300 s^{-1}. Higher concentrations of H_2O result in a decrease in the observed i_{cat}.

The overpotential for the catalytic production of H_2 by $[Ni(8P_2N)_2]^{2+}$ was determined using the method recently reported by Roberts and Bullock,[51] which is based on experimental open circuit measurements at a platinum electrode (eq 7). The $E_{cat/2}$ is defined as the catalytic half-wave potential that corresponds to half the i_{cat} used to determine the turnover frequency (Figure 8b). The thermodynamic equilibrium potential (E_{BH^+}, eq 8) was determined using eq 9, which was established by experimental open circuit measurements.[51] The resulting overpotential for H_2 production by $[Ni(8P_2N)_2]^{2+}$ under dry conditions was determined to be 700 mV at the $E_{cat/2}$, corresponding to the maximum turnover frequency of 800 s^{-1} (0.60 M $(DMF)H^+$). Roberts demonstrated that addition of small amounts of H_2O to $CH_3CN/(DMF)H^+$ solutions affects E_{BH^+} by less than 40 mV, so the same method was used to estimate an overpotential of 760 mV for H_2 production by $[Ni(8P_2N)_2]^{2+}$ under wet conditions (as determined by the $E_{cat/2}$ with 0.82 M $(DMF)H^+$ and 1.1 M H_2O).

dx.doi.org/10.1021/cs400638f | ACS Catal. 2013, 3, 2527−2535

$$\text{overpotential} = |E_{BH^+} - E_{cat/2}| \quad (7)$$

$$DMF(H)^+ + e^- \overset{E_{BH^+}}{\rightleftharpoons} DMF + \frac{1}{2}H_2 \quad (8)$$

$$E_{BH^+} = 0.072 \log([DMF(H)^+]) - 0.192 \quad (9)$$

Computaional Studies. Computational studies on $[Ni(8P_2N)_2]^{2+}$, $[Ni(7P_2N)_2]^{2+}$, and $[Ni(P_2N_2)_2]^{2+}$ were carried out to gain further insights into the properties of the complexes and the catalytic processes as reported below. All calculations were carried out using the free energies of solvation in acetonitrile, which was also explicitly considered as a fifth ligand for all of Ni(II) complexes. The results of these calculations are discussed below.

DISCUSSION

In this work, we investigate the effect of the number of nitrogen atoms within our ligand platforms on the basis of a comparison between $[Ni(8P_2N)_2]^{2+}$ and $[Ni(P_2N_2)_2]^{2+}$; the diphosphine ligands on these two complexes both have 8-membered rings, but the complexes differ in having a total of two or four nitrogen atoms, respectively. We also made comparisons between $[Ni(7P_2N)_2]^{2+}$ and $[Ni(8P_2N)_2]^{2+}$ to determine the effect of the ligand bite angle between the two species. Table 1 summarizes the important structural and electrochemical data of these three complexes.

Table 1. Comparison of Experimental Data for the Three Closely Related Complexes: $[Ni(P_2N_2)_2]^{2+}$, $[Ni(8P_2N)_2]^{2+}$, and $[Ni(7P_2N)_2]^{2+}$

	$[Ni(P_2N_2)_2]^{2+}$ [a]	$[Ni(8P_2N)_2]^{2+}$	$[Ni(7P_2N)_2]^{2+}$ [b]
overpotential[c]	570 mV	760 mV	860 mV
TOF w/o water	740 s^{-1}	800 s^{-1}	6100 s^{-1}
TOF w/water	1040 s^{-1}	3300 s^{-1}	17 000 s^{-1}
Ni (II/I)[d]	−0.79 V	−0.90 V	−1.08 V[c]
Ni (I/0)[d]	−0.97 V	−1.10 V	−1.08 V[e]
P−Ni−P bite angle	82−84°	83°	80°

[a]As previously reported.[47] [b]As previously reported.[8,48,66] [c]For calculated TOF with water as determined by the method of Roberts for calculating overpotentials.[51] [d]All potentials are referenced to the $Cp_2Fe^{+/0}$ couple at 0 V. [e]Overlapping Ni(II/I and I/0) couples.

Analysis of Cyclic Voltammetry. The Ni(I/0) couple for $[Ni(8P_2N)_2]^{2+}$ at −1.10 V occurs very close to the Ni(I/0) couple of $[Ni(7P_2N)_2]^{2+}$ and 130 mV negative of that of $[Ni(P_2N_2)_2]^{2+}$ (Table 1).[8,47] Previous studies have shown the potential of Ni(I/0) couple is more sensitive to electronic effects induced by the ligands than steric effects.[50] Given the structural similarity of the $[Ni(8P_2N)_2]^{2+}$ and $[Ni(P_2N_2)_2]^{2+}$ complexes, the 130 mV difference in their Ni(I/0) couples can be attributed to the electronic effect from replacement of the electron-withdrawing amine group in the ligand backbone with a saturated hydrocarbon. This observation is consistent with previous studies that show replacing the more electronegative N(Me) with a CH_2 in the backbone of the ligand of $[Ni(Et_2PCH_2N(Me)CH_2PEt_2)_2]^{2+}$ compared with $[Ni(Et_2PCH_2CH_2CH_2PEt_2)_2]$ resulted in a 100 mV negative shift in the Ni(I/0) couple.[49]

In previous studies of $[M(diphosphine)_2]^{2+}$ complexes (where M = Ni, Pd, and Pt), the degree of distortion from a square planar geometry has been shown to correlate with the potentials of M(II/I) couples.[50] Specifically, the potentials of the Ni(II/I) couples shift to more positive values as bite angles become larger, facilitating distortion toward a tetrahedral geometry.[50] The single-crystal X-ray structure of $[Ni(8P_2N)_2]^{2+}$ allows for comparison to the previously published $[Ni(P_2N_2)_2]^{2+}$ and $[Ni(7P_2N)_2]^{2+}$ complexes.[8,47] The average P−Ni−P bite angle of 83° in $[Ni(8P_2N)_2]^{2+}$ is nearly identical to those observed in the analogous structures for $[Ni(P^{Ph}{}_2N^{C6H5X}{}_2)_2]^{2+}$ (X = OMe or Me), which range between 82 and 84° (Table 1).[47] The 80° P−Ni−P bite angle observed for $[Ni(7P_2N)_2]^{2+}$, however, is significantly smaller (Table 1).[8] As a result, the potential of the Ni(II/I) couple of $[Ni(8P_2N)_2]^{2+}$ is shifted 200 mV positive of the Ni(I/0) couple. This difference in potentials is consistent with the separation of 180 mV between the Ni(II/I) and Ni(I/0) couples for $[Ni(P_2N_2)_2]^{2+}$, since those complexes presumably have a similar tetrahedral distortion (Table 1).[47]

Computational analysis of the structural, electrochemical, and acid/base properties of $[Ni(8P_2N)_2]^{2+}$, $[Ni(7P_2N)_2]^{2+}$, and $[Ni(P_2N_2)_2]^{2+}$ were carried out, accounting for solvation by CH_3CN, to aid in analysis of the experimental results. The calculated reduction potentials and P−Ni−P bite angles of the complexes are reported in Table 2. The experimentally measured potentials for the Ni(II/I) and (I/0) processes and the calculated potentials for the Ni(II/I) and Ni(I/0) couples are in good agreement.

Table 2. Calculated (and Experimental) Electrochemical Potentials (V) and Calculated P−Ni−P Bite Angle (°) for $[Ni(P_2N_2)_2]^{2+}$, $[Ni(8P_2N)_2]^{2+}$, and $[Ni(7P_2N)_2]^{2+}$ in CH_3CN

	$[Ni(P_2N_2)_2]^{2+}$	$[Ni(8P_2N)_2]^{2+}$	$[Ni(7P_2N)_2]^{2+}$
E(II/I)	−0.84 (−0.79)	−0.94 (−0.90)	−1.06 (−1.08)
E(I/0)	−0.91 (−0.97)	−1.14 (−1.10)	−1.09 (−1.08)
P−Ni−P bite angle	82.0	83.2	78.1

Mechanistic Studies. The proposed mechanism consisting of chemical (C) and electrochemical (E) steps for the formation of H_2 catalyzed by $[Ni(8P_2N)_2]^{2+}$ is illustrated in Figure 9 and is analogous to that previously proposed for the $[Ni(P^R{}_2N^{R'}{}_2)_2]^{2+}$ complexes.[27] The $[Ni(8P_2N)_2]^{2+}$ complexes are first electrochemically reduced (moving clockwise around Figure 9) to the Ni(I) species (ECEC′, step 1), followed by protonation of a pendant amine (ECEC′, step 2_{exo}) and the second electron transfer (ECEC′, step 3) to form the monoprotonated Ni(0) complex $[Ni(8P_2NH)(8P_2N)]^+$. The $[Ni(8P_2NH)(8P_2N)]^+$ complex must then be protonated in an endo position to form the doubly protonated Ni(0) species (ECEC′, step $4_{exo/endo}$), followed immediately by an intramolecular proton transfer from nitrogen to nickel to form a protonated Ni(II) hydride (ECEC′, step 5). The final steps of the mechanism require an intermolecular isomerization to form the Ni(II) proton/hydride complex, followed by H−H bond formation and hydrogen elimination, regenerating the original catalyst (ECEC′, steps 6−8). Although the focus of this discussion is on an ECEC′ mechanism, it is important to note an EECC′ mechanism also likely contributes to the overall measured turnover frequency of the catalytic process (Figure 9, alternative steps $2-3_{exo}$).

After the reduction of Ni(II) to Ni(I) (step 1), protonation on the nitrogen atoms can occur endo to form **e(I)** (**e** indicating endo, **I** indicating the oxidation state of the metal, Supporting Information, Figure S1) or exo to form **x(I)** (**x** indicating exo protonation, Figure 9, step 2_{exo}), with respect to

dx.doi.org/10.1021/cs400638f | ACS Catal. 2013, 3, 2527−2535

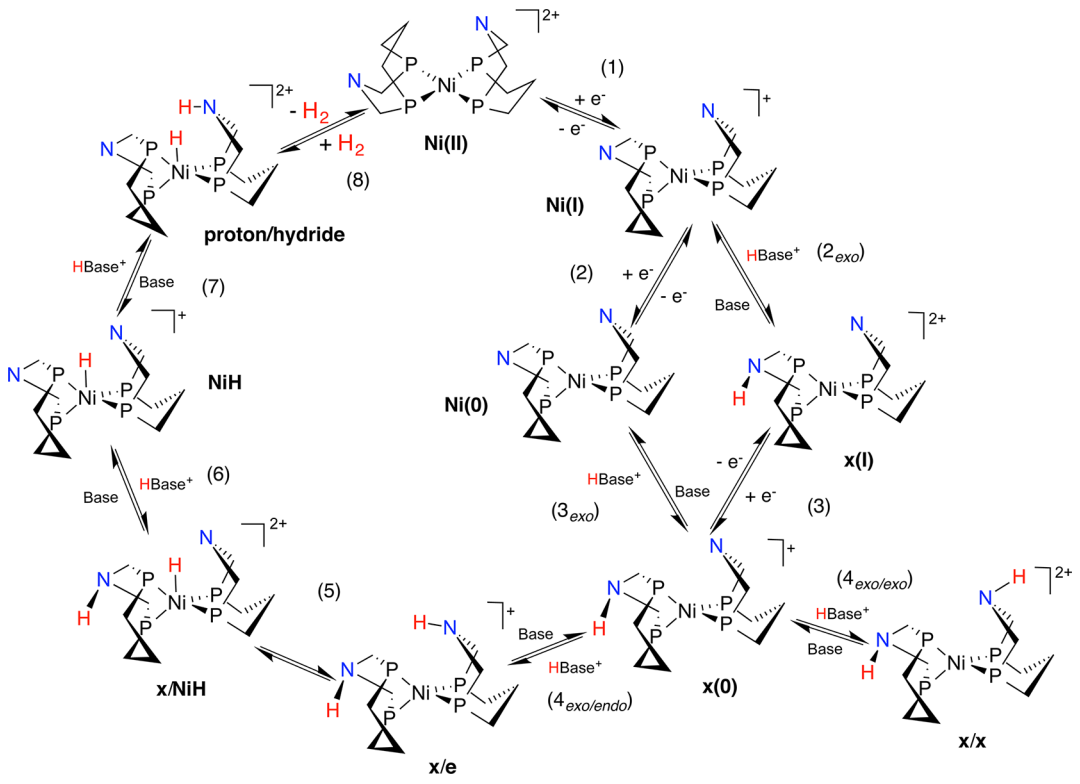

Figure 9. Proposed ECEC′ and EECC′ mechanisms for catalytic H_2 formation (clockwise) by $[Ni(8P_2N)_2]^{2+}$. Aryl substituents on the phosphorus and nitrogen atoms have been omitted for clarity.

the metal center. Protonation to give the **e(I)** isomer would be the preferred catalytic pathway (Supporting Information, Figure S1), requiring fewer steps to reach the Ni(II) proton/hydride species necessary for H_2 evolution. When using $(DMF)H^+$ as the proton source (pK_a = 6.1 in CH_3CN),[59,60] analysis of the catalytic wave for hydrogen production by $[Ni(8P_2N)_2]^{2+}$ reveals a current enhancement near the Ni(II/I) couple (Figure 6), indicating that electrochemical reduction occurs before the first protonation step. The calculated pK_a values and Ni(I/0) potentials for the lowest free-energy isomers of the singly protonated Ni(I) isomers of $[Ni(8P_2NH)(8P_2N)]^{2+}$ are reported in Table 3. The pK_a of the **e(I)** species resulting from reduction and protonation of $[Ni(8P_2N)_2]^{2+}$ is calculated to be less than 1 pK_a unit different from that of the **x(I)** species. In contrast, calculated pK_a values for $[Ni(P_2N_2H)(P_2N_2)]^{2+}$ indicate that protonation of $[Ni(P_2N_2)_2]^{+}$ to give the exo isomer, **x(I)**, is favored over endo protonation (Table 3). Since there is only one pendant amine in each $8P_2N$ ligand, reactions of $[Ni(8P_2N)_2]^{2+}$ cannot form a N···HN hydrogen bond (Figure 2c) that stabilizes the related complexes with P_2N_2 ligands. The lower thermodynamic stability of the exo isomer of $[Ni(8P_2NH)(8P_2N)]^{2+}$ compared with $[Ni(P_2N_2H)(P_2N_2)]^{2+}$ parallels the trend recently reported for the exo isomer of $[Ni(7P_2NH)(7P_2N)]^{2+}$ (Table 3).[8] The similar rates of H_2 production for $[Ni(8P_2N)_2]^{2+}$ and $[Ni(P_2N_2)_2]^{2+}$ relative to the faster catalysis with $[Ni(7P_2N)_2]^{2+}$, however, appear to be due to a combination of formation of unfavorable exo isomers and the weak basicity of the complexes relative to the $(DMF)H^+$ proton source (Table 3). Unlike the large separation in the pK_a values for the singly protonated **e(I)** and **x(I)** isomers of $[Ni(7P_2NH)(7P_2N)]^{2+}$ (>3 pK_a units), the separation of the singly protonated **e(I)** and **x(I)** pK_a values for $[Ni(8P_2NH)(8P_2N)]^{2+}$ is small (about 1 pK_a unit). This implies that protonation to form the **e(I)** and the **x(I)** isomer of $[Ni(8P_2NH)(8P_2N)]^{2+}$ with $[(DMF)H]^+$ are thermodynamically accessible. Previous protonation studies on related $Ni(P^R_2N^{R'}_2)_2$ catalysts have shown that the exo positions are the kinetically preferred sites of protonation.[45,67] Hence, catalysis by the $[Ni(8P_2N)_2]^{2+}$ is thought to proceed through protonation to form the exo isomers.

Table 3. Calculated pK_a Values in CH_3CN for the Ni(I) Protonated Endo, e(I), and Exo, x(I), Isomers of $[Ni(P_2N_2H)(P_2N_2)]^{2+}$, $[Ni(8P_2NH)(8P_2N)]^{2+}$, and $[Ni(7P_2NH)(7P_2N)]^{2+}$

compd	e(I)	x(I)
$[Ni(P_2N_2H)(P_2N_2)]^{2+}$	3.0	4.3
$[Ni(8P_2NH)(8P_2N)]^{2+}$	3.7	2.8
$[Ni(7P_2NH)(7P_2N)]^{2+}$	5.0	1.4

Once formation of the **x(I)** species has occurred, a second reduction to form the **x(0)** complex follows. As mentioned previously, the same species can be reached following an EEC sequence of steps, rather than an ECE process (Figure 9). Protonation of the **x(0)** species can then occur in the endo position to form the **x/e** isomer (Figure 9, step $4_{exo/endo}$) or exo position (Figure 9, step $4_{exo/exo}$) to form the catalytically inactive **x/x** isomer. Previous studies on $[Ni(P^R_2N^{R'}_2)_2]^{2+}$ catalyst revealed the **x/x** species is likely the resting state of the catalyst under operating conditions because the exo protonation site is likely the most kinetically accessible.[67]

Overall, the likely rate-determining steps of the catalytic production of H_2 by $[Ni(8P_2N)_2]^{2+}$ are thought to be dominated by the steady state equilibrium concentration of the monoprotonated **x(0)** isomer with the doubly protonated

dx.doi.org/10.1021/cs400638f | ACS Catal. 2013, 3, 2527−2535

x/**x** isomer (step $4_{exo/exo}$) and the rate of endo protonation of the **x(0)** species (step $4_{exo/endo}$). This conclusion is supported by extensive NMR and computational studies on the related $[Ni(P^R_2N^{R'}_2)_2]^{2+}$ compounds in which the rates of intermolecular proton transfer from the **x**/**x** species to the **e**/**x** species (Figure 9, steps $4_{exo/exo}$ and $4_{exo/endo}$) were found to be slow relative to the following rates of intramolecular proton transfer, isomerization, and H_2 elimination (Figure 9, steps 5−8).[44,45]

These results are consistent with H_2 production by the $[Ni(P_2N_2)_2]^{2+}$ catalysts, in which formation of the **x(I)** isomer is favored by >1 pK_a per unit. The appearance of a second catalytic wave for the production of H_2 by $[Ni(8P_2N)_2]^{2+}$ that shows a plateau near the Ni(I/0) couple of −1.1 V (Figure 7a) suggests an alternative EECC′ pathway may also play a role at more negative potentials. As shown in Figure 9, the rate-determining steps for catalysis by the EECC′ mechanism are likely the same as for the ECEC′ mechanism in which formation of the exo/exo isomer is favored, reducing the concentration of catalyst in the productive catalytic cycle.

Effect of Water on Catalytic Rates. Addition of water (1.0 M) to reaction mixtures containing $[Ni(8P_2N)_2]^{2+}$ complexes and $(DMF)H^+$ results in catalytic rate enhancement from 800 to 3300 s^{-1}, a 4.1-fold increase. The same effect is observed for both $[Ni(P_2N_2)_2]^{2+}$ and $[Ni(7P_2N)_2]^{2+}$, but in the case of $[Ni(P_2N_2)_2]^{2+}$, the observed rate increase is not as large (40% increase).[47,57,68] Previously reported computational and experimental studies suggest the rates of protonation and deprotonation of the pendant amines are hindered through steric interaction between phosphine substituents and the approaching substrate.[39,44,45] In the $[Ni(8P_2N)_2]^{2+}$ complex, water is proposed to function in a similar fashion, increasing the rate of protonation through the ease of access of small water molecules to the pendant amines, thereby shuttling protons from $(DMF)H^+$. The greater enhancement in the catalytic rate upon addition of water to $[Ni(8P_2N)_2]^{2+}$ compared with $[Ni(P_2N_2)_2]^{2+}$ can be attributed to the preferential formation of the **x(I)** species of the later. Experimental and computational work to elucidate the exact role of water in these systems is ongoing in our laboratories.

CONCLUSIONS

The synthesis and electrochemical analysis of $[Ni(8P_2N)_2]^{2+}$ provides a thorough comparison of ligand structural effects and number of pendant amines on the rates of H_2 production by a closely related family of electrocatalysts. Comparisons of $[Ni(8P_2N)_2]^{2+}$ with the $[Ni(7P_2N)_2]^{2+}$ and $[Ni(P_2N_2)_2]^{2+}$ catalysts indicate that the number of pendant amines and their basicity play a crucial role in the rapid delivery of protons to the metal center from the substrate. The similar catalytic rate for H_2 production by $[Ni(8P_2N)_2]^{2+}$ compared with $[Ni(P_2N_2)_2]^{2+}$ can be attributed to formation of noncatalytically productive exo/exo protonated isomers. The data indicate the large difference in the pK_a values favoring endo over exo protonated isomers is important for achieving fast catalytic rates observed with $[Ni(7P_2N)_2]^{2+}$.

EXPERIMENTAL SECTION

General Experimental Procedures. All manipulations with phosphine ligands and metal reagents were carried out under N_2 using standard vacuum line, Schlenk, and inert atmosphere glovebox techniques. Solvents were purified by passage through neutral alumina using an Innovative Technology, Inc., PureSolv solvent purification system. Acetonitrile-d_3 (Cambridge Isotope Laboratories, 99.5%D) was vacuum-distilled from P_2O_5. Chloroform-*d* (Cambridge Isotope Laboratories, 99.5%D) was degassed and stored over molecular sieves. Tetraethylammonium tetrafluoroborate (Alfa-Aesar) was recrystallized twice by vapor diffusion of diethyl ether into an acetonitrile solution; the crystals obtained were dried under vacuum. Water was dispensed from a Millipore Milli-Q purifier and sparged with nitrogen. Ferrocene (Aldrich) was sublimed under vacuum before use. The $[(DMF)H]OTf$,[69] $[Ni(CH_3CN)_6](BF_4)_2$[70] and 1,3-bis(hydroxymethylphenylphosphino)propane[47,56] were prepared by the literature methods.

Instrumentation. NMR spectra were recorded on a Varian spectrometer (500 MHz for ^1H) at 25 °C unless otherwise noted. All ^1H chemical shifts have been internally calibrated using the monoprotio impurity of the deuterated solvent, and $^{31}P\{^1H\}$ NMR spectra were referenced to external phosphoric acid at 0 ppm. Electrospray ionization (ESI) and chemical ionization (CI) mass spectra were collected at the Indiana University Mass Spectrometry Facility on a Waters/Micromass LCT Classic using anhydrous solvents and inert atmosphere techniques.

All electrochemical measurements were conducted in 0.2 M $[NEt_4][BF_4]/CH_3CN$ at 25 °C, under nitrogen in a Vacuum Atmospheres glovebox. A standard three-electrode configuration was employed in conjunction with CH Instruments 660C or 1100A potentiostat interfaced to a computer for data collection. All voltammetric scans were recorded using glassy-carbon working electrode disks of 1 mm diameter encased in PEEK (Cypress Systems EE040). The working electrode was treated between scans by polishing with diamond paste (Buehler) in sequence of decreasing sizes (3 to 0.25 μm) interspersed by washings with purified H_2O (vide infra). A glassy-carbon rod (Structure Probe, Inc.) and silver wire (Alfa-Aesar) were used as auxiliary electrodes and quasi-reference electrodes, respectively. All glassware for electrochemical experiments was oven-dried overnight and allowed to cool under vacuum. Ferrocene was used as an internal standard, and all potentials reported within this work are referenced to the ferrocenium/ferrocene couple at 0 V.

Synthesis of meso-$8P^{Ph}_2N^{C_6H_4Br}$. To a solution of 1,3-bis(hydroxymethylphenylphosphino)-propane (5.00 g, 1.56 mmol) in ∼10 mL toluene and ∼20 mL of ethanol at 70 °C was added *p*-bromoaniline (2.50 g, 1.45 mmol) in 5 mL toluene. The mixture was stirred overnight at 70 °C then concentrated to ∼1/3 volume under vacuum. A white precipitate was collected by filtration and identified by $^{31}P\{^1H\}$ NMR spectroscopy as primarily the rac isomer. The remaining solution was further concentrated until ∼5 mL of solvent remained, and the pure meso isomer was collected as a white solid by filtration. Yield 0.60 g (18%). $^{31}P\{^1H\}$ NMR ($CDCl_3$, 202.2 MHz): δ −31.2 (s). ^1H NMR ($CDCl_3$, 499.7 MHz): δ 7.52 (m, Ar*H*, 4H); 7.39 (m, Ar*H*, 6H); 7.32 (m, Ar*H*, 2H); 6.63 (m, Ar*H*, 4H); 4.184 (m, CH_2, 2H); 3.77 (dd, J_{HH} = 15 Hz, 4 Hz, CH_2, 2H); 2.41 (m, CH_2, 1H); 2.193 (d, J_{HH} = 8 Hz CH_2, 1H); 2.164 (m, CH_2, 2H); 2.09 (m, CH_2, 2H). MS-APCI observed $\{8P_2N^{C_6H_4Br}H\}^+$: 456.065. Calculated for $\{8P_2N^{C_6H_4Br}H\}^+$: 456.065.

Synthesis of $[Ni(8P^{Ph}_2N^{C_6H_4Br})_2](BF_4)_2$. To a stirring solution of $[Ni(CH_3CN)_6](BF_4)_2$ (0.030 g, 0.060 mmol) in 10 mL of CH_3CN at 22 °C, $8P^{Ph}_2N^{C_6H_4Br}$ (0.056 g, 0.12 mmol) was added. The resulting red solution was stirred for 1 h, after

dx.doi.org/10.1021/cs400638f | ACS Catal. 2013, 3, 2527−2535

which diethyl ether (5 mL) was added, resulting in the precipitation of a red solid. The solid was separated from the solution and dried under vacuum. Yield: 0.056 g (78%). $^{31}P\{^{1}H\}$ NMR (CD_3CN, 25 °C, ppm): 4.2 (s), 20.1 (broad), −11.6 (broad). ^{1}H NMR (CD_3CN, 25 °C, ppm): 7.65−7.00 (multiple peaks, 28H, C_6H_5), 4.50−4.30 (mult, 8H, PCH_2N), 3.00−2.06 (mult, 12, CH_2). Observed $\{[Ni(8P^{Ph}{}_2N^{C_6H_4Br})_2](BF_4)\}^+$: 1057.050. Calculated for $\{[Ni(8P^{Ph}{}_2N^{C_6H_4Br})_2](BF_4)\}^+$: 1057.050.

Computational Studies. Computational studies on $[Ni(8P^{Ph}{}_2N^{C_6H_4Br})_2]^{2+}$, $[Ni(7P^{Ph}{}_2N^{C_6H_4Br})_2]^{2+}$ and $[Ni(P^{Ph}{}_2N^{C_6H_4Br}{}_2)_2]^{2+}$ were carried out to gain further insights into the complex properties and the catalytic process. Molecular structures were optimized at the DFT level of theory with the hybrid B3P86[71,72] exchange and correlation functional. Stuttgart−Dresden relativistic ECP and associated basis set[73] was used for Ni, and Pople's 6-31G*, for all nonmetal atoms. Additional polarization *p* function on proton was included. Harmonic vibrational frequencies were calculated at the optimized geometries using the same level of theory to estimate the zero-point energy and the thermal contributions (298 K and 1 atm) to the gas-phase free energy. Free energies of solvation in acetonitrile (which include the change of thermodynamic conditions of P = 1 atm in the gas phase to 1 M solution) were then computed using a self-consistent reaction field model at the same level of theory as for the other steps. The conductor-like polarizable continuum model[74,75] was used with Bondi radii.[76] All geometries were optimized without any symmetry constraint and were verified by vibrational analyses at the same level of theory to ensure that they are minima on the potential energy surface. For some complexes, several conformations were considered, and the lowest energy conformer was chosen for the calculation of the thermodynamic properties. Acetonitrile was explicitly considered as fifth ligand for all Ni(II) complexes. The pK_a values and redox potential were calculated according to the isodesmic scheme discussed by Chen et al.[77] The $[Ni(P^{Cy}{}_2N^{Bn}{}_2H)_2]^{2+}$ system is used as reference for the pK_a calculations, and $[Ni(P^{Ph}{}_2N^{Ph}{}_2)_2]^{2+}$, for the redox potential. All of the calculations were carried out with Gaussian 09.[78]

The selection of the hybrid B3P86 functional and basis set was shown to provide redox potentials, hydride donor strengths, and pK_a values with good accuracy for a set of complexes with various metals and ligands[77] and activation barriers for proton transfer and heterolytic H−H bond formation that compare favorably with CCSD(T) calculations level of theory.[79] However, the computational error due to the exchange and correlation functional and the continuum solvation model adopted can be as large as 2−3 kcal/mol.[46,79,80]

■ ASSOCIATED CONTENT

Ⓢ Supporting Information

Electrocatalysis studies, alternative EECC catalytic pathway, and crystal information. This material is available free of charge via the Internet at http://pubs.acs.org.

■ AUTHOR INFORMATION

Corresponding Author

*E-mail: Monte.Helm@pnnl.gov.

Notes

The authors declare no competing financial interest.

■ ACKNOWLEDGMENTS

We thank Dr. Jonathan M. Darmon and Dr. Charles J. Weiss for their assistance with the graphical abstract. This research was supported as part of the Center for Molecular Electrocatalysis, an Energy Frontier Research Center funded by the U.S. Department of Energy, Office of Science, Basic Energy Sciences. Pacific Northwest National Laboratory is operated by Battelle for the U.S. Department of Energy.

■ REFERENCES

(1) Lewis, N. S.; Nocera, D. G. *Proc. Natl. Acad. Sci. U.S.A.* **2006**, *103*, 15729−15735.
(2) Conway, B. E.; Bockris, J. O. *J. Chem. Phys.* **1956**, *26*, 532−541.
(3) Trasatti, S. In *Modern Chlor-Alkali Technology*; Wellington, T. C., Ed.; Springer: Netherlands, 1992; Vol. *45*, pp 281−294−4202.
(4) Laursen, A. B.; Kegnæs, S.; Dahl, S.; Chorkendorff, I. *Energy Environ. Sci.* **2012**, *5*, 5577−5591.
(5) Popczun, E. J.; McKone, J. R.; Read, C. G.; Biacchi, A. J.; Wiltrout, A. M.; Lewis, N. S.; Schaak, R. E. *J. Am. Chem. Soc.* **2013**, *135*, 9267−9270.
(6) Nocera, D. G. *Acc. Chem. Res.* **2012**, *45*, 767−776.
(7) Wang, M.; Chen, L.; Sun, L. *Energy Environ. Sci.* **2012**, *5*, 6763−6778.
(8) Stewart, M. P.; Ho, M.-H.; Wiese, S.; Lindstrom, M. L.; Thogerson, C. E.; Raugei, S.; Bullock, R. M.; Helm, M. L. *J. Am. Chem. Soc.* **2013**, *135*, 6033−6046.
(9) *Catalysis without Precious Metals*, 1st ed.; Bullock, R. M., Ed.; Wiley-VCH: Weinheim, 2010.
(10) Thoi, V. S.; Sun, Y.; Long, J. R.; Chang, C. J. *Chem. Soc. Rev.* **2013**, *42*, 2388−2400.
(11) Frey, M. *ChemBioChem* **2002**, *3*, 153−160.
(12) Vincent, K. A.; Parkin, A.; Armstrong, F. A. *Chem. Rev.* **2007**, *107*, 4366−4413.
(13) Armstrong, F. A.; Hirst, J. *Proc. Natl. Acad. Sci. U.S.A.* **2011**, *108*, 14049−14054.
(14) Cracknell, J. A.; Vincent, K. A.; Armstrong, F. A. *Chem. Rev.* **2008**, *108*, 2439−2461.
(15) Nicolet, Y.; Piras, C.; Legrand, P.; Hatchikian, C. E.; Fontecilla-Camps, J. C. *Structure* **1999**, *7*, 13−23.
(16) Nicolet, Y.; de Lacey, A. L.; Vernède, X.; Fernandez, V. M.; Hatchikian, E. C.; Fontecilla-Camps, J. C. *J. Am. Chem. Soc.* **2001**, *123*, 1596−1601.
(17) Silakov, A.; Wenk, B.; Reijerse, E.; Lubitz, W. *Phys. Chem. Chem. Phys.* **2009**, *11*, 6592−6599.
(18) Peters, J. W.; Lanzilotta, W. N.; Lemon, B. J.; Seefeldt, L. C. *Science* **1998**, *282*, 1853−1858.
(19) Ott, S.; Kritikos, M. M.; Akermark, B. B.; Sun, L.; Lomoth, R. *Angew. Chem., Int. Ed.* **2004**, *43*, 1006−1009.
(20) Schwartz, L.; Eilers, G. G.; Eriksson, L. L.; Gogoll, A. A.; Lomoth, R.; Ott, S. *Chem. Commun.* **2006**, 520−522.
(21) Schwartz, L.; Ekström, J.; Lomoth, R.; Ott, S. *Chem. Commun.* **2006**, 4206−4208.
(22) Jiang, S. S.; Liu, J. J.; Shi, Y. Y.; Wang, Z. Z.; Akermark, B. B.; Sun, L. *Dalton Trans.* **2007**, 896−902.
(23) Barton, B. E.; Olsen, M. T.; Rauchfuss, T. B. *J. Am. Chem. Soc.* **2008**, *130*, 16834−16835.
(24) van der Vlugt, J. I.; Rauchfuss, T. B.; Whaley, C. M.; Wilson, S. R. *J. Am. Chem. Soc.* **2005**, *127*, 16012−16013.
(25) Lawrence, J. D.; Li, H.; Rauchfuss, T. B.; Bénard, M.; Rohmer, M.-M. *Angew. Chem., Int. Ed.* **2001**, *40*, 1768−1771.
(26) Singleton, M. L.; Crouthers, D. J.; Duttweiler, R. P.; Reibenspies, J. H.; Darensbourg, M. Y. *Inorg. Chem.* **2011**, *50*, 5015−5026.
(27) Shaw, W. J.; Helm, M. L.; DuBois, D. L. *Biochim. Biophys. Acta, Bioenerg.* **2013**, *1827*, 1123−1139.
(28) DuBois, D. L.; Bullock, R. M. *Eur. J. Inorg. Chem.* **2011**, *2011*, 1017−1027.

(29) Le Goff, A.; Artero, V.; Jousselme, B.; Tran, P. D.; Guillet, N.; Métayé, R.; Fihri, A.; Palacin, S.; Fontecave, M. *Science* **2009**, *326*, 1384−1387.
(30) Stubbert, B. D.; Peters, J. C.; Gray, H. B. *J. Am. Chem. Soc.* **2011**, *133*, 18070−18073.
(31) Artero, V.; Chavarot-Kerlidou, M.; Fontecave, M. *Angew. Chem., Int. Ed.* **2011**, *50*, 7238−7266.
(32) Jacques, P.-A.; Artero, V.; Pecaut, J.; Fontecave, M. *Proc. Natl. Acad. Sci. U.S.A.* **2009**, *106*, 20627−20632.
(33) Dempsey, J. L.; Brunschwig, B. S.; Winkler, J. R.; Gray, H. B. *Acc. Chem. Res.* **2009**, *42*, 1995−2004.
(34) Rose, M. J.; Gray, H. B.; Winkler, J. R. *J. Am. Chem. Soc.* **2012**, *134*, 8310−8313.
(35) Liu, X.; Ibrahim, S. K.; Tard, C.; Pickett, C. J. *Coord. Chem. Rev.* **2005**, *249*, 1641−1652.
(36) Gloaguen, F.; Rauchfuss, T. B. *Chem. Soc. Rev.* **2009**, *38*, 100−108.
(37) Tard, C.; Pickett, C. J. *Chem. Rev.* **2009**, *109*, 2245−2274.
(38) Camara, J. M.; Rauchfuss, T. B. *Nat. Chem.* **2012**, *4*, 26−30.
(39) Liu, T.; DuBois, D. L.; Bullock, R. M. *Nat. Chem.* **2013**, *5*, 228−233.
(40) Liu, T.; Chen, S.; O'Hagan, M. J.; Rakowski DuBois, M.; Bullock, R. M.; DuBois, D. L. *J. Am. Chem. Soc.* **2012**, *134*, 6257−6272.
(41) Appel, A. M.; DuBois, D. L.; Rakowski DuBois, M. *J. Am. Chem. Soc.* **2005**, *127*, 12717−12726.
(42) Karunadasa, H. I.; Chang, C. J.; Long, J. R. *Nature* **2010**, *464*, 1329−1333.
(43) Karunadasa, H. I.; Montalvo, E.; Sun, Y.; Majda, M.; Long, J. R.; Chang, C. J. *Science* **2012**, *335*, 698−702.
(44) O'Hagan, M. J.; Shaw, W. J.; Raugei, S.; Chen, S.; Yang, J. Y.; Kilgore, U. J.; DuBois, D. L.; Bullock, R. M. *J. Am. Chem. Soc.* **2011**, *133*, 14301−14312.
(45) O'Hagan, M. J.; Ho, M.-H.; Yang, J. Y.; Appel, A. M.; Rakowski DuBois, M.; Raugei, S.; Shaw, W. J.; DuBois, D. L.; Bullock, R. M. *J. Am. Chem. Soc.* **2012**, *134*, 19409−19424.
(46) Raugei, S.; Chen, S.; Ho, M.-H.; Ginovska-Pangovska, B.; Rousseau, R. J.; Dupuis, M.; DuBois, D. L.; Bullock, R. M. *Chem.—Eur. J.* **2012**, *18*, 6493−6506.
(47) Kilgore, U. J.; Roberts, J. A. S.; Pool, D. H.; Appel, A. M.; Stewart, M. P.; Rakowski DuBois, M.; Dougherty, W. G.; Kassel, W. S.; Bullock, R. M.; DuBois, D. L. *J. Am. Chem. Soc.* **2011**, *133*, 5861−5872.
(48) Helm, M. L.; Stewart, M. P.; Bullock, R. M.; Rakowski DuBois, M.; DuBois, D. L. *Science* **2011**, *333*, 863−866.
(49) Curtis, C. J.; Miedaner, A.; Ciancanelli, R.; Ellis, W. W.; Noll, B. C.; Rakowski DuBois, M.; DuBois, D. L. *Inorg. Chem.* **2003**, *42*, 216−227.
(50) Berning, D. E.; Noll, B. C.; DuBois, D. L. *J. Am. Chem. Soc.* **1999**, *121*, 11432−11447.
(51) Roberts, J. A. S.; Bullock, R. M. *Inorg. Chem.* **2013**, *52*, 3823−3835.
(52) Berning, D. E.; Miedaner, A.; Curtis, C. J.; Noll, B. C.; Rakowski DuBois, M.; DuBois, D. L. *Organometallics* **2001**, *20*, 1832−1839.
(53) Raebiger, J. W.; Miedaner, A.; Curtis, C. J.; Miller, S. M.; Anderson, O. P.; DuBois, D. L. *J. Am. Chem. Soc.* **2004**, *126*, 5502−5514.
(54) Fraze, K.; Wilson, A. D.; Appel, A. M.; Rakowski DuBois, M.; DuBois, D. L. *Organometallics* **2007**, *26*, 3918−3924.
(55) Miedaner, A.; Haltiwanger, R. C.; DuBois, D. L. *Inorg. Chem.* **1991**, *30*, 417−427.
(56) Karasik, A. A.; Naumov, R. N.; Spiridonova, Y. S.; Sinyashin, O. G.; Lönnecke, P.; Hey-Hawkins, E. *Z. Anorg. Allg. Chem.* **2007**, *633*, 205−210.
(57) Kilgore, U. J.; Stewart, M. P.; Helm, M. L.; Dougherty, W. G.; Kassel, W. S.; Rakowski DuBois, M.; DuBois, D. L.; Bullock, R. M. *Inorg. Chem.* **2011**, *50*, 10908−10918.
(58) Bard, A. J.; Faulkner, L. R. *Electrochemical Methods: Fundamentals and Applications*; 2nd ed. Wiley: New York, 2000.
(59) Kolthoff, I. M.; Chantooni, M. K.; Bhowmik, S. *Anal. Chem.* **1967**, *39*, 1627−1633.
(60) Izutsu, K. *Acid-Base Dissociation Constants in Dipolar Aprotic Solvents*; Blackwell Scientific Publications: Oxford, Boston, 1990.
(61) Nicholson, R. S.; Shain, I. *Anal. Chem.* **1964**, *36*, 706−723.
(62) Savéant, J. M.; Vianello, E. *Electrochim. Acta* **1965**, *10*, 905−920.
(63) Savéant, J. M.; Vianello, E. *Electrochim. Acta* **1967**, *12*, 629−646.
(64) Savéant, J. M. *Chem. Rev.* **2008**, *108*, 2348−2378.
(65) Savéant, J. M. *Acc. Chem. Res.* **1980**, *13*, 323−329.
(66) Hoffert, W. A.; Roberts, J. A. S.; Bullock, R. M.; Helm, M. L. *Chem. Commun.* **2013**, *49*, 7767−7769.
(67) Appel, A. M.; Pool, D. H.; O'Hagan, M. J.; Shaw, W. J.; Yang, J. Y.; Rakowski DuBois, M.; DuBois, D. L.; Bullock, R. M. *ACS Catal.* **2011**, *1*, 777−785.
(68) Wiese, S.; Kilgore, U. J.; DuBois, D. L.; Bullock, R. M. *ACS Catal.* **2012**, *2*, 720−727.
(69) Favier, I.; Duñach, E. *Tetrahedron Lett.* **2004**, *45*, 3393−3395.
(70) Hathaway, B. J.; Holah, D. G.; Underhill, A. E. *J. Chem. Soc.* **1962**, 2444−2448.
(71) Perdew, J. P. *Phys. Rev. B* **1986**, *33*, 8822−8824.
(72) Becke, A. D. *J. Chem. Phys.* **1993**, *98*, 5648.
(73) Andrae, D.; Häußermann, U.; Dolg, M.; Stoll, H.; Preuß, H. *Theor. Chim. Acta* **1990**, *77*, 123−141.
(74) Cossi, M.; Rega, N.; Scalmani, G.; Barone, V. *J. Comput. Chem.* **2003**, *24*, 669−681.
(75) Barone, V.; Cossi, M. *J. Phys. Chem. A* **1998**, *102*, 1995−2001.
(76) Bondi, A. *J. Phys. Chem.* **1964**, *68*, 441−451.
(77) Chen, S.; Rousseau, R. J.; Raugei, S.; Dupuis, M.; DuBois, D. L.; Bullock, R. M. *Organometallics* **2011**, *30*, 6108−6118.
(78) Frisch, M. J.; Trucks, G. W.; Schlegel, H. B.; Scuseria, G. E.; Robb, M. A.; Cheeseman, J. R.; Scalmani, G.; Barone, V.; Mennucci, B.; Petersson, G. A.; Nakatsuji, H.; Caricato, M.; Li, X.; Hratchian, H. P.; Izmaylov, A. F.; Bloino, J.; Zheng, G.; Sonnenberg, J. L.; Hada, M.; Ehara, M.; Toyota, K.; Fukuda, R.; Hasegawa, J.; Ishida, M.; Nakajima, T.; Honda, Y.; Kitao, O.; Nakai, H.; Vreven, T.; Montgomery, J. A.; Peralta, J. E.; Ogliaro, F.; Bearpark, M.; Heyd, J. J.; Brothers, E.; Kudin, K. N.; Staroverov, V. N.; Kobayashi, R.; Normand, J.; Raghavachari, K.; Rendell, A.; Burant, J. C.; Iyengar, S. S.; Tomasi, J.; Cossi, M.; Rega, N.; Millam, J. M.; Klene, M.; Knox, J. E.; Cross, J. B.; Bakken, V.; Adamo, C.; Jaramillo, J.; Gomperts, R.; Stratmann, R. E.; Yazyev, O.; Austin, A. J.; Cammi, R.; Pomelli, C.; Ochterski, J. W.; Martin, R. L.; Morokuma, K.; Zakrzewski, V. G.; Voth, G. A.; Salvador, P.; Dannenberg, J. J.; Dapprich, S.; Daniels, A. D.; Farkas; Foresman, J. B.; Ortiz, J. V.; Cioslowski, J.; Fox, D. J. *Gaussian 09, Revision B01*, Gaussian, Inc.: Wallingford. CT, 2009.
(79) Chen, S.; Raugei, S.; Rousseau, R. J.; Dupuis, M.; Bullock, R. M. *J. Phys. Chem. A* **2010**, *114*, 12716−12724.
(80) Liakos, D. G.; Hansen, A.; Neese, F. *J. Chem. Theory Comput.* **2011**, *7*, 76−87.